articles

molecular pharmaceutics

Real Time, Noninvasive Imaging and Quantitation of the Accumulation of Ligand-Targeted Drugs into Receptor-Expressing Solid Tumors

Erina Vlashi,[†] Jennifer E. Sturgis,[‡] Mini Thomas,[†] and Philip S. Low*[,†]

Department of Chemistry and Bindley Bioscience Center, Purdue University, West Lafayette, Indiana 47907

Received June 25, 2009; Revised Manuscript Received September 4, 2009; Accepted September 14, 2009

Abstract: Targeted therapies are emerging as a preferred strategy for treatment of cancer and other diseases. To evaluate the effect of high affinity receptors on the rate and extent of tumor penetration of receptor-targeted drugs, we have characterized the kinetics of folate−rhodamine uptake by folate receptor (FR)-expressing tumors in live mice. Folate−rhodamine was selected to model receptor-targeted drugs, because (i) it has high affinity ($K_d = 10^{-9}$ M) for FR-rich tumors, (ii) its uptake can be monitored *in vivo* by multiphoton microscopy, and (iii) five folate-targeted drugs of similar size are currently undergoing clinical trials. We demonstrate that (1) folate−rhodamine saturates tumor FR in <5 min, <30 min, and <100 min following intravenous, paraorbital, and intraperitoneal injection, respectively; (2) complete clearance of folate−rhodamine from receptor-negative tissues requires ≥50 min, and (3) a "binding site barrier" may retard, but does not prevent, penetration of the ligand-targeted drug. We conclude that low molecular weight ligand-targeted drugs have appropriate pharmacokinetic properties for tumor-selective delivery.

Keywords: Targeted cancer therapy; folic acid; real time imaging; tumor uptake

Introduction

Most chemotherapeutic agents cause damage to malignant and healthy cells alike, resulting in dose-limiting toxicities that compromise the therapeutic potential of the drug. To avoid these toxicities, the design of targeted anticancer agents that concentrate their lethal activities specifically in cancer tissues has been undertaken.[1] Two distinct classes of such targeted therapeutics are now in the clinic: (i) inhibitors that are specific for enzymes/processes uniquely important for cancer cell survival and/or proliferation, and (ii) nonspecific cytotoxic drugs that achieve tumor specificity by virtue of their attachment to targeting ligands that bind selectively to cancer cells. Examples of the former class of targeted pharmaceuticals include low molecular weight drugs such as imatinib (Gleevec),[2,3] gefitinib (Iressa),[4] and erlotinib (Tarceva),[5] and monoclonal antibodies like trastuzumab (Herceptin),[6,7] rituximab (Rituxin) and bevacizumab (Avastin).[8,9] Examples of the latter class of ligand-targeted agents are Mylotarg, a monoclonal antibody to CD33 antigen linked to calicheamicin[10] and a fusion of pseudomonas exotoxin (PE38) and IL-2 that is targeted to IL-2R overexpressing malignant cells.[11,12]

Although greatly benefited by improved tumor specificity, protein and monoclonal antibody-targeted drugs are simul-

* Corresponding author. Mailing address: Purdue University, Department of Chemistry, 560 Oval Drive, West Lafayette, IN 47907-2084. E-mail: plow@purdue.edu. Phone: 765-494-5273. Fax: 765-494-5272.

† Department of Chemistry.

‡ Bindley Bioscience Center.

(1) Ross, J. S.; Schenkein, D. P.; Pietrusko, R.; et al. Targeted therapies for cancer 2004. *Am. J. Clin. Pathol.* **2004**, *122*, 598–609.

(2) Arslan, M. A.; Kutuk, O.; Basaga, H. Protein kinases as drug targets in cancer. *Curr. Cancer Drug Targets* **2006**, *6*, 623–34.

(3) Mauro, M. J.; Druker, B. J. STI571: a gene product-targeted therapy for leukemia. *Curr. Oncol. Rep.* **2001**, *3*, 223–7.

(4) Kirby, A. M.; A'Hern, R. P.; D'Ambrosio, C.; et al. Gefitinib (ZD1839, Iressatrade mark) as palliative treatment in recurrent or metastatic head and neck cancer. *Br. J. Cancer* 2006.

10.1021/mp900158d CCC: $40.75
Published on Web 09/15/2009

taneously compromised by poor tumor penetration due to their large sizes.[13] To avoid this limitation, a new class of low molecular weight targeting ligands has emerged that penetrate tumors more efficiently. Although no member of this class has achieved FDA approval, several are in clinical trials, including folic acid-,[14−18] vitamin B12-,[19,20] bombesin-,[21,22] LHRH-,[23,24] and GnRH-linked drugs,[25,26] all of which bind receptors that are overexpressed on a population of human tumors.

While several studies describing the rate and magnitude of tumor penetration of nontargeted cancer drugs have been published,[13,27−30] no information is available on the pharmacokinetics of tumor penetration of ligand-targeted drugs. Although questions regarding the effect of receptor density and affinity and tumor vascularization have been addressed in the context of tumor specific antibodies, such questions remain to be addressed in the context of ligand-targeted drug delivery. Further, the hypothesis that a "binding site barrier" may exist[31−34]—where the first few ligand-targeted drug molecules with high affinity for a tumor cell surface receptor that escape the vasculature and bind to receptors on immediately adjacent cancer cells retard the penetration of subsequent conjugates, due to the "sink" effect—remains to be tested with small targeted drugs.

To begin to address the impact of a high affinity ligand on the rate and depth of tumor penetration of a ligand-targeted drug, we designed a model system composed of folic acid linked to rhodamine. Folic acid was selected as the targeting ligand, since it binds the folate receptor (FR) with

(5) Blackhall, F. H.; Rehman, S.; Thatcher, N. Erlotinib in non-small cell lung cancer: a review. *Expert Opin. Pharmacother.* **2005**, *6*, 995–1002.
(6) Arnould, L.; Gelly, M.; Penault-Llorca, F.; et al. Trastuzumab-based treatment of HER2-positive breast cancer: an antibody-dependent cellular cytotoxicity mechanism. *Br. J. Cancer* **2006**, *94*, 259–67.
(7) Romond, E. H.; Perez, E. A.; Bryant, J.; et al. Trastuzumab plus adjuvant chemotherapy for operable HER2-positive breast cancer. *N. Engl. J. Med.* **2005**, *353*, 1673–84.
(8) Blagosklonny, M. V. How avastin potentiates chemotherapeutic drugs: action and reaction in antiangiogenic therapy. *Cancer Biol. Ther.* **2005**, *4*, 1307–10.
(9) Gasparini, G.; Longo, R.; Toi, M.; Ferrara, N. Angiogenic inhibitors: a new therapeutic strategy in oncology. *Nat. Clin. Pract. Oncol.* **2005**, *2*, 562–77.
(10) Sievers, E. L.; Linenberger, M. Mylotarg: antibody-targeted chemotherapy comes of age. *Curr. Opin. Oncol.* **2001**, *13*, 522–7.
(11) Kawakami, K.; Nakajima, O.; Morishita, R.; Nagai, R. Targeted anticancer immunotoxins and cytotoxic agents with direct killing moieties. *TheScientificWorld* **2006**, *6*, 781–90.
(12) Kreitman, R. J.; Pastan, I. Targeting Pseudomonas exotoxin to hematologic malignancies. *Semin. Cancer Biol.* **1995**, *6*, 297–306.
(13) Dreher, M. R.; Liu, W.; Michelich, C. R.; Dewhirst, M. W.; Yuan, F.; Chilkoti, A. Tumor vascular permeability, accumulation, and penetration of macromolecular drug carriers. *J. Natl. Cancer Inst.* **2006**, *98*, 335–44.
(14) Leamon, C. P.; Low, P. S. Selective targeting of malignant cells with cytotoxin-folate conjugates. *J. Drug Targeting* **1994**, *2*, 101–12.
(15) Ross, J. F.; Chaudhuri, P. K.; Ratnam, M. Differential regulation of folate receptor isoforms in normal and malignant tissues in vivo and in established cell lines. Physiologic and clinical implications. *Cancer* **1994**, *73*, 2432–43.
(16) Toffoli, G.; Cernigoi, C.; Russo, A.; Gallo, A.; Bagnoli, M.; Boiocchi, M. Overexpression of folate binding protein in ovarian cancers. *Int. J. Cancer* **1997**, *74*, 193–8.
(17) Lu, Y.; Sega, E.; Leamon, C. P.; Low, P. S. Folate receptor-targeted immunotherapy of cancer: mechanism and therapeutic potential. *Adv. Drug Delivery Rev.* **2004**, *56*, 1161–76.
(18) Hilgenbrink, A. R.; Low, P. S. Folate receptor-mediated drug targeting: from therapeutics to diagnostics. *J. Pharm. Sci.* **2005**, *94*, 2135–46.
(19) Huennekens, F. M.; DiGirolamo, P. M.; Fujii, K.; Jacobsen, D. W.; Vitols, K. S. B12 -- dependent methionine synthetase as a potential target for cancer chemotherapy. *Adv. Enzyme Regul.* **1976**, *14*, 187–205.
(20) Bagnato, J. D.; Eilers, A. L.; Horton, R. A.; Grissom, C. B. Synthesis and characterization of a cobalamin-colchicine conjugate as a novel tumor-targeted cytotoxin. *J. Org. Chem.* **2004**, *69*, 8987–96.
(21) Stangelberger, A.; Schally, A. V.; Letsch, M.; et al. Targeted chemotherapy with cytotoxic bombesin analogue AN-215 inhibits growth of experimental human prostate cancers. *Int. J. Cancer* **2006**, *118*, 222–9.
(22) Szepeshazi, K.; Schally, A. V.; Nagy, A.; Halmos, G. Inhibition of growth of experimental human and hamster pancreatic cancers in vivo by a targeted cytotoxic bombesin analog. *Pancreas* **2005**, *31*, 275–82.
(23) Nagy, A.; Schally, A. V. Targeting cytotoxic conjugates of somatostatin, luteinizing hormone-releasing hormone and bombesin to cancers expressing their receptors: a "smarter" chemotherapy. *Curr. Pharm. Des.* **2005**, *11*, 1167–80.
(24) Dharap, S. S.; Wang, Y.; Chandna, P.; et al. Tumor-specific targeting of an anticancer drug delivery system by LHRH peptide. *Proc. Natl. Acad. Sci. U.S.A.* **2005**, *102*, 12962–7.
(25) Eaveri, R.; Ben-Yehudah, A.; Lorberboum-Galski, H. Surface antigens/receptors for targeted cancer treatment: the GnRH receptor/binding site for targeted adenocarcinoma therapy. *Curr. Cancer Drug Targets* **2004**, *4*, 673–87.
(26) Ben-Yehudah, A.; Lorberboum-Galski, H. Targeted cancer therapy with gonadotropin-releasing hormone chimeric proteins. *Expert Rev. Anticancer Ther.* **2004**, *4*, 151–61.
(27) Ahmed, A. E.; Jacob, S.; Giovanella, B. C.; Kozielski, A. J.; Stehlin, J. S., Jr.; Liehr, J. G. Influence of route of administration on [3H]-camptothecin distribution and tumor uptake in CASE-bearing nude mice: whole-body autoradiographic studies. *Cancer Chemother. Pharmacol.* **1996**, *39*, 122–30.
(28) Noy, R.; Ben-Zvi, Z.; Elezra, M.; et al. Pharmacokinetics and organ distribution of N-methanocarbathymidine, a novel thymidine analog, in mice bearing tumors transduced with the herpes simplex thymidine kinase gene. *Cancer Chemother. Pharmacol.* **2002**, *50*, 360–6.
(29) Harivardhan Reddy, L.; Sharma, R. K.; Chuttani, K.; Mishra, A. K.; Murthy, R. S. Influence of administration route on tumor uptake and biodistribution of etoposide loaded solid lipid nanoparticles in Dalton's lymphoma tumor bearing mice. *J. Controlled Release* **2005**, *105*, 185–98.
(30) Minchinton, A. I.; Tannock, I. F. Drug penetration in solid tumours. *Nat. Rev. Cancer* **2006**, *6*, 583–92.

high affinity ($K_d \sim 10^{-9}$ M) and because FR is overexpressed on a large fraction of human cancers.[15,35−38] Rhodamine was chosen as a surrogate drug, since its concentration can be quantitated noninvasively *in vivo* in real time using multiphoton intravital fluorescence microscopy.

Experimental Procedures

Materials. Fmoc-protected amino acid derivatives, Fmoc-Lys(Mtt)-loaded Wang resin, 2-(1*H*-benzotriazol-1-yl)-1,1,3,3-tetramethyluronium hexafluorophosphate (HBTU), and *N*-hydroxybenzotriazole (HOBT) were purchased from Novabiochem (San Diego, CA). N^{10}-Trifluoroacetylpteroic acid was synthesized from folic acid (Sigma, St. Louis, MO) as described previously.[39] Rhodamine B-isothiocyanate was purchased from SIGMA (St. Louis, MO). Nude mice and folate-deficient chow were purchased from Harlan (Indianapolis, IN). Sources of other chemicals are described in the text.

Synthesis of Folate−Rhodamine. Standard Fmoc peptide chemistry was used to conjugate folate to rhodamine B-isothiocyanate via the γ-COOH terminal of folic acid. Lys-(γ)Glu-pteroic acid was initially constructed using Fmoc chemistry with HBTU and HOBT as the activating agents and diisopropylethylamine (DIPEA) as the base. The Fmoc groups were deprotected with 20% piperidine in dimethylformamide (DMF). Wang resin loaded with α-Fmoc-protected lysine containing a 4-methyltrityl protecting group on the ε-amine was used to attach Fmoc-Glu-O*t*Bu to the α-amine of the lysine, after removal of the Fmoc-group, and to provide a γ-linked conjugate of folate after N^{10}-trifluoroacetylpteroic acid was attached to the amine of glutamic acid. The methoxytrityl protecting group on the ε-amine of lysine was removed with 1% trifluoroacetic acid in dichloromethane (DCM), and rhodamine B-isothiocyanate dissolved in DMF was reacted overnight with the peptide in the presence of DIPEA. After thorough washing of the beads, the folate−rhodamine peptide conjugate was cleaved from the resin with 95% trifluoroacetic acid−2.5% water−2.5% triisopropylsilane solution for 3−4 h. Ice cold diethyl ether was used to precipitate the product, and the precipitant was collected by centrifugation. The product was washed three times with diethyl ether and was dried under vacuum. The product was then resuspended in water, and concentrated ammonium hydroxide was added until the pH of the solution reached 10. The solution was stirred for 30 min at room temperature and then lyophilized and purified by HPLC, as previously described.[40] The pure product was collected, lyophilized and resuspended in phosphate buffered saline (PBS) for animal studies. Mass spectroscopy analysis ([M$^-$] calculated, 1069; found, 1068) was in agreement with the expected structure.

***In Vivo* Animal Model.** Nude mice (BALB/c *nu/nu*) between 6 and 7 weeks of age were placed on a folate-deficient diet (Harlan Diet T00434; Harlan Teklad) for 2 weeks in order to reduce serum folate concentrations to near human physiological levels (∼15 nmol/L).[41] FR-positive KB cells (a malignant human nasopharygeal cell line) and FR-negative A549 cells (human lung adenocarcinoma epithelial cell line) were cultured at 37 °C in a humidified atmosphere containing 5% CO_2 in air. The cells were grown continuously as a monolayer in folate-deficient RPMI 1640 medium (Gibco BRL, Gaithersburg, MD) supplemented with 10% fetal bovine serum (Hyclone Laboratories, Logan, UT), penicillin (50 units/mL), and streptomycin (50 μg/mL) (SIGMA, St. Louis, MO). The normal complement of endogenous folates in the fetal bovine serum elevates the folate concentration in the growth medium to near the physiological range found in human plasma. For tumor implantation, cells were dislodged using Cell Dissociation Solution (Gibco BRL, Gaithersburg, MD) and resuspended in folate-deficient RPMI 1640 medium at a concentration of 10 million cells/mL. One million KB, or A549 cells, suspended in 100 μL of RPMI media, were implanted intradermally on the four legs of *nu/nu* mice to grow very superficial solid tumors of approximately 5−6 mm in diameter. This model afforded relatively hair-free, superficial

(31) Fujimori, K.; Covell, D. G.; Fletcher, J. E.; Weinstein, J. N. A modeling analysis of monoclonal antibody percolation through tumors: a binding-site barrier. *J. Nucl. Med.* **1990**, *31*, 1191–8.
(32) Juweid, M.; Neumann, R.; Paik, C.; et al. Micropharmacology of monoclonal antibodies in solid tumors: direct experimental evidence for a binding site barrier. *Cancer Res.* **1992**, *52*, 5144–53.
(33) Weinstein, J. N.; van Osdol, W. Early intervention in cancer using monoclonal antibodies and other biological ligands: micropharmacology and the "binding site barrier". *Cancer Res.* **1992**, *52*, 2747s–51s.
(34) Saga, T.; Neumann, R. D.; Heya, T.; et al. Targeting cancer micrometastases with monoclonal antibodies: a binding-site barrier. *Proc. Natl. Acad. Sci. U.S.A.* **1995**, *92*, 8999–9003.
(35) Campbell, I. G.; Jones, T. A.; Foulkes, W. D.; Trowsdale, J. Folate-binding protein is a marker for ovarian cancer. *Cancer Res.* **1991**, *51*, 5329–38.
(36) Weitman, S. D.; Lark, R. H.; Coney, L. R.; et al. Distribution of the folate receptor GP38 in normal and malignant cell lines and tissues. *Cancer Res.* **1992**, *52*, 3396–401.
(37) Wu, M.; Gunning, W.; Ratnam, M. Expression of folate receptor type alpha in relation to cell type, malignancy, and differentiation in ovary, uterus, and cervix. *Cancer Epidemiol. Biomarkers Prev.* **1999**, *8*, 775–82.
(38) Parker, N.; Turk, M. J.; Westrick, E.; Lewis, J. D.; Low, P. S.; Leamon, C. P. Folate receptor expression in carcinomas and normal tissues determined by a quantitative radioligand binding assay. *Anal. Biochem.* **2005**, *338*, 284–93.
(39) Luo, J. S. M.; Lantrip, D. A.; Wang, S.; Fuchs, P. L. Efficient syntheses of pyrofolic acid and pteroyl azide, reagents for the production of carboxyl-differentiated derivatives of folic acid. *J. Am. Chem. Soc.* **1997**, *119*, 10004–13.
(40) Henne, W. A.; Doorneweerd, D. D.; Hilgenbrink, A. R.; Kularatne, S. A.; Low, P. S. Synthesis and activity of a folate peptide camptothecin prodrug. *Bioorg. Med. Chem. Lett.* **2006**, *16*, 5350–5.
(41) Mathias, C. J.; Wang, S.; Lee, R. J.; Waters, D. J.; Low, P. S.; Green, M. A. Tumor-selective radiopharmaceutical targeting via receptor-mediated endocytosis of gallium-67-deferoxamine-folate. *J. Nucl. Med.* **1996**, *37*, 1003–8.

solid tumors, which allowed visualization of the tumor vasculature and tumor-associated folate−rhodamine fluorescence in a noninvasive manner (through the skin), using a multiphoton microscope. During imaging, the mice were anesthetized with a ketamine/xylazine (Lloyd Laboratories, Shenandoah, IA) cocktail (100/10 mg/kg, intraperitoneally). All animal experiments were performed in accordance with Purdue University's institutional animal care and use committee guidelines.

Injection of Fluorescent Probes. Two hours before imaging, the mice (∼20 g) were injected with 1 mg of Hoechst 33342 intraperitoneally to label cell nuclei. Immediately before imaging, each mouse was placed in a mouse restrainer and a catheter (Braintree Scientific Inc.) was implanted in the lateral tail vein. Each catheter, filled with heparin solution (100 U/mL), was fixed in place with Vetbond skin adhesive after insertion. The vasculature of the mouse was labeled by intravenous administration of 1 mg (in 100 μL) of PBS fluorescein labeled 2 MDa dextran (Molecular Probes, Eugene, Oregon). The appropriate amount of folate−rhodamine solution was mixed with PBS to a final volume of 100 μL, and injected via the tail vein catheter when the iv administration route was being analyzed. Alternatively, 100 μL of folate−rhodamine was administered intraperitoneally, or through the paraorbital space of the eye. The functional blood vessels were identified by the apparent movement of the blood cells, which appear black as a result of excluding the fluorescent dextran, within the blood vessel. In order to make the interpretation of the data as simple as possible, we identified and focused on blood vessels that appeared isolated from others. Labeling of the vasculature with dextran−FITC allowed the visualization of blood vessels as deep as ∼80 μm from the surface of the skin.

Microscopy. All tumor imaging was conducted using a Bio-Rad Radiance 2100MP Rainbow (Hemmel Hemstead, England) attached to a Nikon TE2000 inverted microscope (Tokoyo, Japan) with a Nikon 60× 1.2 NA water-immersion objective. Multiphoton excitation was provided by a Mai Tai tunable, femtosecond pulsed, titanium-sapphire laser (Spectra-Physics, Mountain View, CA). The fluorescence of the folate−rhodamine, dextran−FITC, and Hoechst 33352 were collected simultaneously. Excitation at 800 nm was found to be optimal for excitation of all three fluorochromes. The same excitation wavelength and power and PMT gain were used in all studies. Each image comprised a field of view of 205 × 205 μm. Images were collected at 512 × 512 pixels with a scan speed of 500 lines per second.

A 50 mm #1.5 coverslip-bottomed dish (World Precision Instruments, Sarasota Florida) was secured to a custom-made plastic stage insert. After the tail vein catheter was secured in place and the mouse was anesthetized, the tumor was positioned flat onto the coverslip-bottomed cell culture dish, already wet with phosphate buffered saline. A heating pad was then placed over the animal to maintain body temperature, and the tumor was centered in the field of view. The green fluorescence of the tumor vasculature was localized first with a 10× objective, and then the objective was changed to 60×. After identifying and focusing on a functional blood vessel, folate−rhodamine was injected into the tail vein catheter, and time series images were collected for the first 5 min at the rate of 1 image every 5 s. After this initial collection period, images were collected every few minutes until the fluorescence of rhodamine in the tumor tissue reached apparent saturation. Blood vessels that were clearly isolated from other blood vessels were selected for imaging in order to simplify analysis of the data. Two or three animals were used for each experiment, and standard error means are presented as error bars.

Image Processing. Metamorph Image Processing Software (Universal Imaging, West Chester, PA) was used to produce time-lapse movies and z-series projections. The colors shown in the figures are similar to the "true" colors of probe fluorescence. Each frame of a time series was analyzed for the intensity of rhodamine at different distances from the blood vessel using ImageJ software (http://rbs.info.nih-gov/ij/). The intensity of rhodamine was determined by quantitating the fluorescence of the selected pixels in the red channel (arbitrary units). Rhodamine intensity was then plotted against the time point corresponding to each frame. Prism (GraphPad Prism version 4.03 for Windows, GraphPad Software, San Diego, CA, www.graphpad.com) was used to fit the data points to known equations.

Results

The Experimental Model. Uptake of folate−rhodamine by KB tumor xenografts (a human nasopharyngeal cancer cell line) implanted on athymic nude mice was used as a model system to characterize the rate and extent of penetration of ligand-targeted drugs into receptor-rich solid tumors. For this purpose, solid tumors were grown intradermally on the shoulders and thighs of nude mice, and after intravenous injection of folate−rhodamine to label FR-positive cells and Hoechst dye to stain nuclei, a z-scan of the KB tumor (a series of images extending progressively deeper through the skin into the tumor) was obtained. As seen in Figure 1 (panels 1−3), two distinct staining patterns are observed. After lowering the plane of focus through the epidermis, normal skin cells (panels 1 and 2 and part of panel 3) are characterized by well-ordered nuclei (labeled blue) and an absence of folate−rhodamine. However, as the focal plane is lowered further until it enters the tumor, cell nuclei become disorganized (characteristic of malignant tissue) and accumulation of folate−rhodamine becomes prominent (Figure 1, panels 4−8). Importantly, in mice injected solely with Hoechst dye, no red fluorescence is detectable in any tissue, including tumor tissue (Figure 3A, top left square), suggesting that tissue autofluorescence does not interfere with quantitation of folate−rhodamine. Because folate−rhodamine fluorescence was also absent from normal tissues (except kidneys) in folate−rhodamine injected mice, we conclude that administration of folate−rhodamine to KB tumor-bearing nude mice constitutes a useful model for characterizing the pharmacokinetics of folate−targeted drug uptake by a receptor-rich solid tumor.

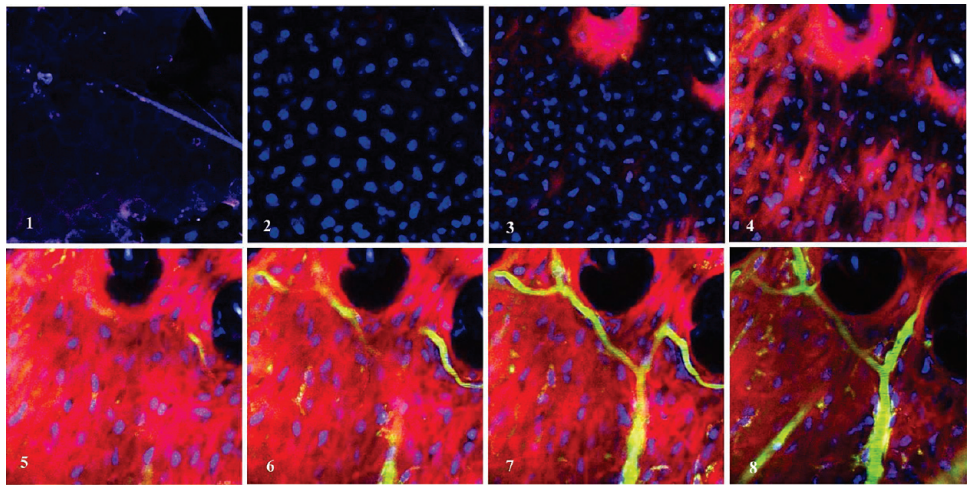

Figure 1. Selective staining of FR+ tumor tissue following tail vein paraorbital injection of folate−rhodamine. An intradermal KB tumor was grown on the thigh to ∼5 mm diameter prior to paraorbital folate−rhodamine (500 nmol/kg) injection. Serial z-section images were collected 1 h after injection. The first few layers of the tissue (panels 1−3) are normal skin and therefore do not retain folate−rhodamine, whereas the subcutaneous tissue is malignant and therefore accumulates folate−rhodamine (red color, panels 4−8). Blood vessels appear green due to intravenous injection of dextran−FITC (MW 2M). Cell nuclei are labeled blue by intraperitoneal administration of Hoechst 33342.

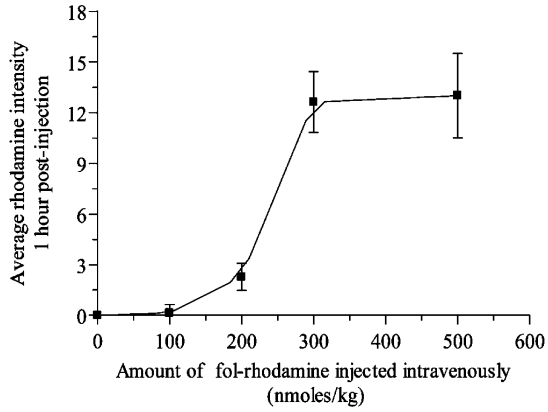

Figure 2. Analysis of the concentration dependence of tumor uptake of folate−rhodamine. Different doses of folate−rhodamine were administered intravenously (100, 200, 300, 500 nmol/kg), and final rhodamine intensity in the tissue was determined 1 h later (n = 3 for each dose).

Dose Dependent Saturation of the Solid Tumor. In order to determine the dose of targeted drug necessary to saturate FR in KB tumors, different doses of folate−rhodamine were administered intravenously and tumor accumulation was monitored over time using the methods described above. A saturating dose was identified by plotting rhodamine intensity in the tumor versus dose administered. As seen in Figure 2, folate−rhodamine uptake by the tumor appeared to saturate at a dose of ∼300 nmol/kg. However, to avoid unwanted variations in pharmacokinetics due to possible localized differences in FR levels, a dose of 500 nmol/kg was used for all subsequent studies.

Pharmacokinetics of Folate−Rhodamine Accumulation in FR+ Solid Tumors. Next, we analyzed the effect that route of administration might have on the kinetics of tumor saturation. For this purpose, three distinct sites of folate−rhodamine injection were compared: intravenous (iv), paraorbital (po), and intraperitoneal (ip). A representative chronological series of images collected at the same tumor site following paraorbital injection is shown in Figure 3A. At the time of folate−rhodamine administration (time 0 min), blood vessels appear green due to the presence of previously injected dextran−fluorescein that was introduced to label the vasculature. Within ∼5 s, however, the vasculature turns yellow due to the appearance of folate−rhodamine and its colocalization with dextran−fluorescein in the same vessel. By ∼10 s postinjection, colocalization of the two fluorescent dyes in the vasculature is maximal (i.e., all blood vessels appear yellow), after which a gradual return of green fluorescence is seen as the folate−rhodamine enters the tissues, leaving the impermeable dextran−fluorescein to mark the blood vessels. Over the next ∼30 min, folate−rhodamine intensity in the tumor slowly increases as empty FRs become occupied by circulating and interstitial folate−rhodamine.

In Figure 3B the kinetics of tumor accumulation are quantitated following each of the aforementioned routes of administration. Although maximal accumulation appears to be largely independent of the site of folate−rhodamine injection, the rate of tumor saturation is very route dependent. Thus, the tumor mass appears to saturate in <5 min when the conjugate is administered iv (tail vein), in <30 min when administered po, and <100 min when injected ip (Figure 3B). We hypothesize these injection route differences primarily reflect the different rates at which folate−rhodamine moves from the site of injection into the bloodstream.

To begin to assess the impact of high affinity FR on the magnitude and kinetics of tumor accumulation of a saturating dose of folate−rhodamine, the kinetics of folate−rhodamine uptake were compared between tumors that contained and tumors that lacked FR. For analysis of tumors that lacked available FR, either all FR were blocked in KB tumors by

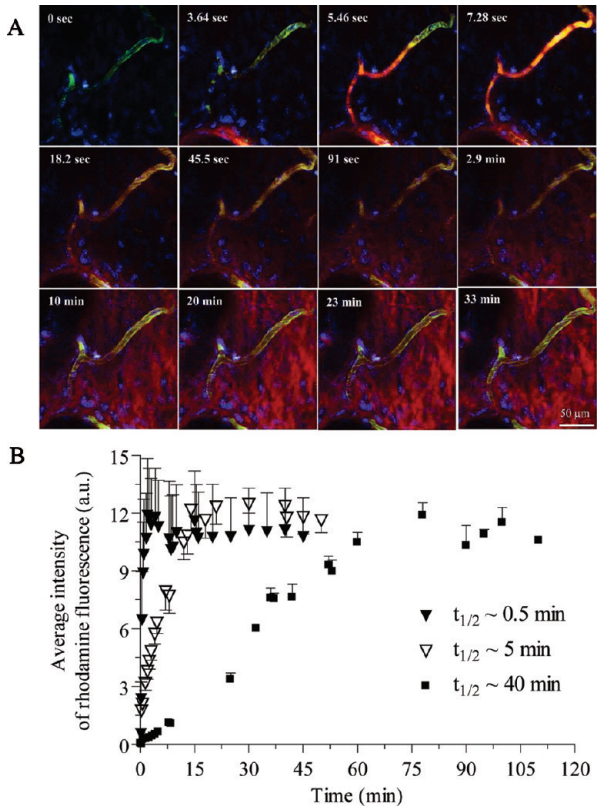

Figure 3. (A) Time course of uptake of folate−rhodamine by tumor tissue following paraorbital administration of the conjugate. Tumor vasculature was labeled green by prior intravenous administration of dextran−FITC (MW 2M), and cell nuclei were labeled blue by prior administration of Hoechst dye 33342. As folate−rhodamine enters the bloodstream, its red fluorescence combined with the green dextran fluorescence results in a yellow color that gradually returns to green as the folate−rhodamine clears from the bloodstream. As folate−rhodamine is captured by receptors in the tumor, red fluorescence gradually increases. (B) Analysis of the kinetics of folate−rhodamine uptake as a function of route of administration. Folate−rhodamine (500 nmol/kg) was administered intravenously (solid triangles), paraorbitally (open triangles), or intraperitoneally (solid squares) and uptake into tumor tissue was monitored as a function of time. Half-times for tumor saturation are indicated in the figure ($n = 3$).

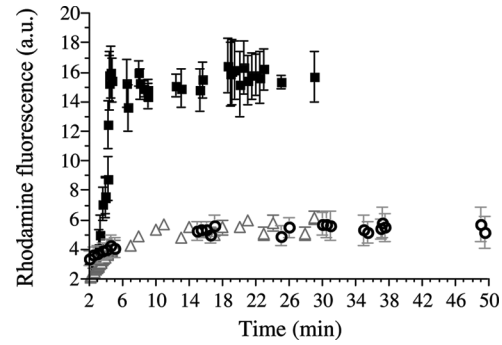

Figure 4. Effect of folate receptor density on the kinetics of folate−rhodamine penetration and uptake into tumor tissue. The kinetics of folate−rhodamine uptake was monitored in unmodified KB tumors (solid squares), FR-negative A549 tumors (solid, gray triangles), and KB tumors presaturated with 100-fold molar excess of folic acid to block empty FR (open circles) ($n = 2-3$).

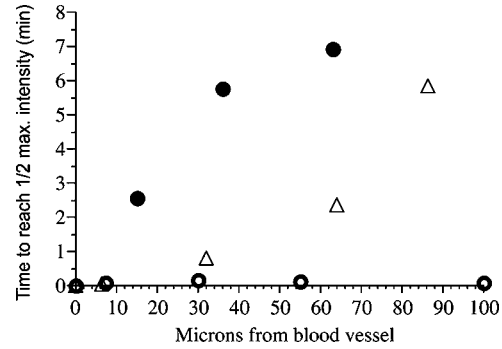

Figure 5. Evaluation of a "binding site barrier" to tumor penetration of folate−rhodamine. Rhodamine intensity was quantified (au) as a function of time at different distances from the nearest blood vessel and the time required to reach half maximal intensity (1/2 I_{max}) was determined. Two different doses of folate−rhodamine were evaluated in KB tumors with accessible FRs (solid symbols): saturation dose of 500 nmol/kg (solid triangles) and subsaturating dose of 300 nmol/kg (solid circles). KB tumors lacking FRs, due to prior blocking of FR with 100-fold excess free folic acid (open circles), were assayed similarly.

preinjection of a saturating dose of free folic acid (100× the concentration of folate−rhodamine) or a tumor that expresses no measurable FR (A547 cell line) was used. Folate−rhodamine was then injected into the tail vein of the tumor-bearing mouse, and uptake was quantitated at a site ~60 μm from the nearest capillary. While the kinetics of tumor accumulation of folate rhodamine varied somewhat from site to site within a tumor mass (probably due to differences in vasculature permeability or tumor organization), the initial rate of penetration of folate−rhodamine into tumors lacking available FR was roughly comparable to its initial rate of penetration into tumors containing unoccupied FR (Figure 4). However, the amount of conjugate retained in the tumors was significantly different, with the FR-saturated tumors and FR-negative tumors capturing only a fraction as much folate conjugate as the tumors with unoccupied FR (Figure 4).

To look for the possible existence of a "binding site barrier" that might impede conjugate penetration into FR-rich solid tumors, we analyzed the time required to reach half maximal fluorescence intensity at different distances from the nearest blood vessel. As shown in Figure 5, penetration of folate−rhodamine into receptor-deficient tumors (modeled by saturating all FR with 100-fold excess free folic acid) occurred rapidly, reaching all cells in the tumor mass in <1 min. In contrast, penetration of the conjugate into FR-rich tumors was transiently retarded, especially to distances >30 μm. Moreover, this delay in

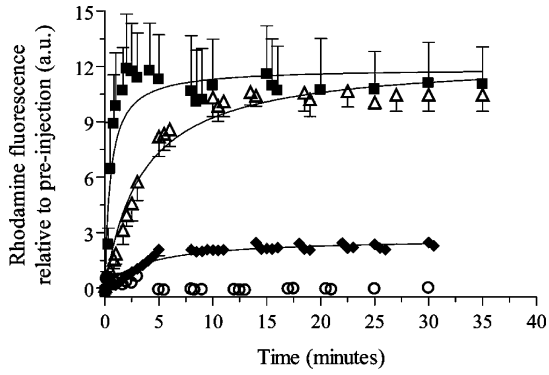

Figure 6. Kinetics of tumor uptake of folate−rhodamine as a function of dose administered. Different concentrations of folate−rhodamine, 100 (open circles), 200 (solid diamonds), 300 (open triangles) and 500 (solid squares) nmol/kg, were injected and accumulation in intradermal KB tumors at a distance of ~50 to 80 μm from the nearest blood vessel was monitored as a function of time ($n = 2-3$).

penetration to distal FR was concentration dependent, with an increase in retardation at lower folate conjugate concentrations (Figure 5). These data suggest that conjugate binding to proximal FR may slightly retard conjugate penetration to more distal FR (see also time lapse video clip in Supporting Information). Nevertheless, at least with a conjugate the size of folate−rhodamine, the impact of the observed "binding site barrier" on drug delivery appears to be transient, since the half time for saturation of even the most distant FR is only a few minutes and eventually all FR appear to become saturated. Indeed, thin sections taken through the centers of nonnecrotic tumors show a uniform distribution of folate−rhodamine across the entire tumor mass, suggesting that the binding site barrier does not constitute a permanent obstacle to drug penetration (Supplementary Figure 1 in the Supporting Information).

Finally, to examine the effect of folate−rhodamine concentration on its kinetics of accumulation in an FR-rich tumor, we monitored the tumor uptake of different doses of the targeted fluorophore. As seen in Figure 6, as increasing concentrations of folate−rhodamine (i.e., 100, 200, 300, 500 nmol/kg) are injected via the tail vein, the time required to reach maximal tumor uptake decreases. Presumably, the higher diffusion potential associated with higher doses of conjugate promotes faster penetration of the interstitial spaces, as also seen in Figure 5.

Discussion

It has been hypothesized that high affinity interactions between tumor antigens and antibodies (or ligands) might impair tumor penetration of the latter and thereby diminish antibody targeting *in vivo*.[32−34,42,43] Thus, when the dynamics of tumor penetration and accumulation of high affinity antibodies were analyzed in the late 1980s, a "binding site barrier" hypothesis was formulated to describe the effect of antibody affinity on their penetration and accumulation into solid tumors. Because folate conjugates have similar affinities with much smaller sizes than tumor-targeted antibodies (M_r ~150,000 versus <1000), it was not obvious whether the low molecular weight folate conjugates might also experience a "binding site barrier" during tumor perfusion. To address this issue, we quantitated the uptake kinetics of folate−rhodamine in tumors enriched and depleted of unoccupied FR. Although some variability existed among different tumors, we observed that even with a targeted "drug" as small as rhodamine a weak "binding site barrier" does exist. However, in contrast to the barrier seen with antibodies, the impediment to tumor penetration was only temporary, since all FR eventually became saturated with folate conjugate. Thus, after an initial delay, the spatial distribution of folate−rhodamine became homogeneous throughout the entire tumor (Figures 1 and 3A), even at distances as far as ~150 μm from the nearest blood vessel (Figure 3A, scale bar 50 μm). It will be important in the future to determine at what conjugate size a binding site barrier converts from a temporary delay to a permanent impediment to tumor penetration. At that size threshold, one might anticipate targeted therapeutics to begin to decline in therapeutic potency.

When folate conjugates are not captured by an unoccupied FR, they can only contribute to nonspecific toxicity. Therefore, it is important to determine the dose of folate−targeted drug necessary to saturate tumor tissue *in vivo*. To determine this saturating dose, escalating concentrations of folate−rhodamine were administered intravenously into tumor bearing mice and the final tumor-associated rhodamine fluorescence was quantified. Although a saturating dose of ~300 nmol/kg was determined (Figure 2), the sigmoidal shape of the saturation curve was not anticipated. A possible explanation for this phenomenon might be that some normal tissues express very low levels of FR that will compete for circulating folate conjugates until their FR are saturated. Once FR on normal organs are saturated, all remaining folate conjugates should be free to saturate tumor FR.[44]

A recent study by Scopinaro et al.[45] has demonstrated that a ^{99m}Tc-labeled bombesin conjugate, which is cleared rapidly from the plasma, must reach its tumor destination within 15 min to achieve optimal tumor imaging. Folate−drug conjugates that are designed to release their therapeutic cargo only

(42) van Osdol, W.; Fujimori, K.; Weinstein, J. N. An analysis of monoclonal antibody distribution in microscopic tumor nodules: consequences of a "binding site barrier". *Cancer Res.* **1991**, *51*, 4776–84.

(43) Graff, C. P.; Wittrup, K. D. Theoretical analysis of antibody targeting of tumor spheroids: importance of dosage for penetration, and affinity for retention. *Cancer Res.* **2003**, *63*, 1288–96.

(44) Kennel, S. J. Effects of target antigen competition on distribution of monoclonal antibody to solid tumors. *Cancer Res.* **1992**, *52*, 1284–90.

(45) Scopinaro, F.; Di Santo, G. P.; Tofani, A.; et al. Fast cancer uptake of 99mTc-labelled bombesin (99mTc BN1). *In Vivo* **2005**, *19*, 1071–6.

after uptake by malignant cells[40,46,47] can also be unstable during prolonged circulation, raising the need to know the time required for them to saturate a tumor. Because different routes of drug administration are used in the clinic, we decided to examine the impact that site of injection can exert on rate of accumulation in an FR^+ tumor. Not surprisingly, the most efficient route of administration was intravenous, where tumor sites were saturated in <5 min. Next in efficiency was paraorbital injection (<30 min), followed by intraperitoneal administration (<100 min) (Figure 3B). Taken together with the observation that tumor accumulation is accelerated as saturating doses of conjugate are approached (Figure 6), it can be argued that unstable folate conjugates should be administered intravenously at higher concentrations in order to minimize metabolism prior to tumor entry.

To our knowledge, this is the first report of a real time visualization and quantitation of the uptake of a ligand-targeted drug into a solid tumor *in vivo*. Traditional studies aimed at analyzing drug pharmacokinetics have required removal of blood/tissue samples at periodic time intervals following drug administration. Where real time fluorescence analyses have been employed, window chambers have been implanted over the tumors to permit direct observation of drug uptake.[13,48] While such experimental setups afford real time imaging, surgically implanted window chambers can also cause inflammation leading to increased vascular permeability and emigration of white blood cells, thus complicating interpretation of the data. In our approach, no incision was required, allowing visualization of the tumor in its natural environment, thus providing a "real-life" view of the penetration and accumulation process. It will now be important to employ these methods to understand the penetration and accumulation of folate conjugates of much larger sizes to determine at which cargo size a "binding site barrier" may become relevant.

Supporting Information Available: Figure depicting representative fluorescence and phase contrast images of KB tumor sections and a time lapse video clip of uptake of folate-rhodamine by a KB tumor. This material is available free of charge via the Internet at http://pubs.acs.org.

MP900158D

(46) Leamon, C. P.; Reddy, J. A.; Vlahov, I. R.; et al. Synthesis and biological evaluation of EC72: a new folate-targeted chemotherapeutic. *Bioconjugate Chem.* **2005**, *16*, 803–11.

(47) Vlahov, I. R.; Santhapuram, H. K.; Kleindl, P. J.; Howard, S. J.; Stanford, K. M.; Leamon, C. P. Design and regioselective synthesis of a new generation of targeted chemotherapeutics. Part 1: EC145, a folic acid conjugate of desacetylvinblastine monohydrazide. *Bioorg. Med. Chem. Lett.* **2006**, *16*, 5093–6.

(48) Brown, E.; McKee, T.; diTomaso, E.; et al. Dynamic imaging of collagen and its modulation in tumors in vivo using second-harmonic generation. *Nat. Med.* **2003**, *9*, 796–800.